Huang et al. Journal of Nanobiotechnology (2025) 23:236
https://doi.org/10.1186/s12951-025-03276-3

Journal of Nanobiotechnology

RESEARCH Open Access

Diselenide-based nanoparticles enhancing the radioprotection to the small intestine of mice

Yichi Huang[1], Jiaze Li[1], Sen Wang[1], Hongqi Tian[2*], Saijun Fan[1*] and Yu Zhao[1*]

Abstract

The widespread application of ionizing radiation (IR) in medicine, while beneficial, also poses potential risks that necessitate effective countermeasures. Both 2-(3-aminopropylamino) ethanethiol (WR-1065) and curcumin are recognized as radioprotective agents; however, their clinical utility is hindered by notable shortcomings that could be addressed through reactive oxygen species (ROS)-responsive amphiphilic nanomaterials. We introduced a newly synthesized poly (ethylene glycol) (PEG)-polycaprolactone (PCL) polymer integrated with diselenide bonds and curcumin (HOOC-SeSe-Cur-PEG-SeSe-Cur-PCL, PEG-Cur-SeSe-PCL). The resulting spherical nanoparticles (NPs), which self-assembled from this polymer, were uniform with an average diameter of 118 nm. As a carrier for WR-1065, these NPs demonstrated a loading capacity of 30.9% and an efficacy of 56.7%. Importantly, the degradation of WR-1065 within the NPs was minimal in gastric fluid, decreasing by only approximately 20% over a 6-hour period. The innovative aspect of these NPs is their design to destabilize in ROS-rich environments, facilitating the release of WR-1065 and curcumin. Indeed, the survival rate of mice increased to 50% when these NPs were orally administered prior to exposure to a lethal dose of whole-body irradiation (8 Gy). The radioprotective impact of WR-1065-loaded NPs was evident in the small intestine of irradiated mice, characterized by the amelioration of radiation-induced epithelial damage, reduction of DNA damage, and inhibition of the apoptotic pathway. Collectively, this oral nanocarrier system for WR-1065 and curcumin holds promise as a potential candidate for the prophylaxis and treatment of acute intestinal injuries induced by IR.

*Correspondence:
Hongqi Tian
tianhq@binjiangpharma.com
Saijun Fan
fansaijun@irm-cams.ac.cn
Yu Zhao
zhaoyu@irm-cams.ac.cn

Full list of author information is available at the end of the article

Graphical Abstract

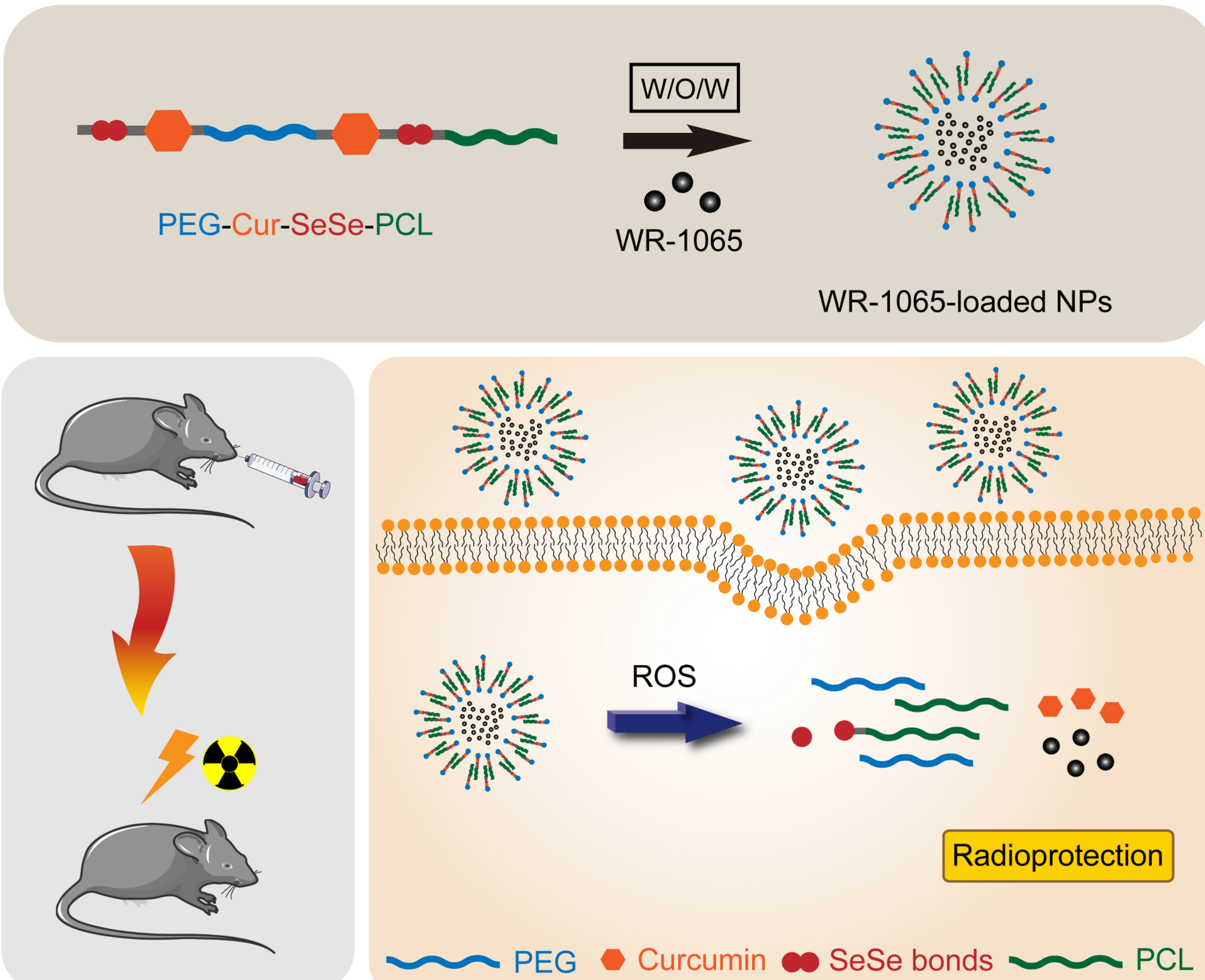

Keywords Ionizing radiation, WR-1065, Curcumin, Nanoparticles, Acute intestine injury

Background

The progress in nuclear and radiation technologies has been remarkable, allowing for their integration into various fields such as industry, agriculture, aerospace, military, and pharmaceutical science [1, 2]. However, the misuse or accidents involving these technologies pose a significant risk of exposure to high-dose ionizing radiation (IR), which can cause the acute damage to healthy tissues and organs particularly the small intestine and hematopoietic systems, potentially leading to acute radiation syndrome (ARS) [3, 4]. IR is known to physically destroy DNA molecules, generate excessive reactive oxygen species (ROS), and disrupt cell homeostasis [5, 6]. Despite these risks, there remains a lack of effective countermeasure to protect individuals from the harmful effect of IR.

Amifostine (WR-2721), the only systemic cytoprotective agent approved by the Food and Drug Administration (FDA), is currently used to shield normal tissues in patients undergoing radiation or chemotherapy [7]. It works through its active metabolite, WR-1065, which is produced by the body after the prodrug amifostine is metabolized [8]. However, the clinical use of amifostine is hindered by its inability to be taken orally and short half-life [9, 10]. Curcumin, a polyphenol derived from turmeric rhizomes (*Curcuma longa L.*), has been reported to offer protection against radiation-induced injuries to various organs and tissues [11–15]. It is valued for its bioactivity and low toxicity, yet its application is limited by properties such as poor water solubility, low bioavailability, instability in physiological conditions, and rapid metabolism in the hepar [16].

In recent years, the medical field has shown increasing interest in stimuli-responsive nanoparticles (NPs) for drug delivery systems (DDS) due to their ability to enhance drug stability, prolong half-life, enhance drug accumulation at targets, and offer new methods of drug administration [17–19]. The surge of ROS production in irradiated areas of the body makes it a viable strategy to effectively deliver WR-1065 and curcumin to these targeted regions using ROS-sensitive materials [20]. Diselenide bonds (Se-Se bonds) with low bond energy of around 172 kJ/mol, are particularly noteworthy for their ease of oxidation or reduction in a redox environment and characterized as a compelling choice for ROS-responsive linking groups in DDS [21, 22]. The application of diselenide-containing nanocarriers for the delivery of anticancer drugs has been documented in existing literature, demonstrating the potential of these bonds to facilitate targeted drug release in response to specific biological triggers [23–25]. However, the study of DDS based on Se-Se bonds in the field of radiation protection remains largely unexplored.

In this study, a novel ROS-responsive and curcumin-linked amphiphilic polymer (HOOC-SeSe-Cur-PEG-Cur-SeSe-PCL, PEG-Cur-SeSe-PCL) was designed and fabricated via a six-step reaction. Utilizing an innovative double emulsion-solvent evaporation technique, we successfully encapsulated WR-1065 within this polymer to form spherical NPs (WR-1065-loaded NPs) that exhibit uniform dispersion. Subsequently, the stability in the simulated gastric environment and sensitivity to ROS of these NPs were evaluated in vitro. Furthermore, we conducted the investigations into the radioprotective capabilities of WR-1065-loaded NPs and the underlying mechanisms in the small intestine of mice after irradiation. The findings from our research indicate that the oral administration of nanomaterial, loaded with WR-1065 and curcumin, holds substantial promise as a radioprotective agent, contributing to the prevention and treatment strategies for acute radiation injuries (ARI).

Methods

Materials and reagents

3-Bromopropionic acid and selenium powder were purchased from J&K Scientific Technology Co. Ltd. (Beijing, China). Poly (ethylene glycol) (PEG, Mn 2000) and polycaprolactone diol (PCL, Mn 2000) were supplied from Macklin Biochemical Co. Ltd. (Shanghai, China). Sodium borohydride ($NaBH_4$), succinic anhydride, curcumin, 1-hydroxybenzotriazole (HOBt), 4-dimethylaminopyridine (DMAP), WR-1065, and ferrous sulfate ($FeSO_4$) were obtained from Ouhe Technology Co. Ltd. (Beijing, China). 1-(3-Dimethylaminopropyl)-3-ethylcarbodiimide hydrochloride (EDCI) and hydrogen peroxide solution (H_2O_2, 30%) were provided by Bide Pharmatech Ltd. (Shanghai, China) and Kemiou Chemical Reagent Co. Ltd. (Tianjin, China), respectively. All the solvents were from Jiangtian Chemical Technology Co. Ltd. (Tianjin, China). All antibodies were purchased from Abcam (Cambridge, UK), CST (Boston, USA), or Proteintech (Chicago, USA).

Animals

Male C57BL/6J mice (6-8 weeks old) were supplied by HFK Bioscience Co. Inc. (Beijing, China) and fed at the SPF Laboratory Animal Center of the Institute of Radiation Medicine (IRM), Chinese Academy of Medical Sciences (CAMS).

Preparation of the polymer

Synthesis of HOOC-PEG-COOH (PEG-COOH)

PEG (5 g, 2.5 mmol) and succinic anhydride (0.55 g, 5.5 mmol) were dissolved in toluene (25 mL) to form a pellucid solution. Then the solution was refluxed under a nitrogen atmosphere at 120℃ for an hour. Once the solvent was removed under a reduced pressure, the residue was heated to 140 ℃ under the protection of nitrogen overnight. After naturally cooling to room temperature, dichloromethane (DCM, 4 mL) was used to dissolve the white solid. Next, the solution was added dropwise to diethyl ether (100 mL) while stirring at 0 ℃ for 3 h. The precipitated product was filtered and dried to obtain a white powder (88% yield).

Synthesis of Cur-PEG-Cur (PEG-Cur)

EDCI (0.60 g, 3.15 mmol) and HOBt (0.43 g, 3.15 mmol) were both placed in the solution of PEG-COOH (3.31 g, 1.5 mmol) in dimethylformamide (DMF, 25 mL). After stirring at room temperature for an hour, curcumin (1.66 g, 4.5 mmol) was introduced to the reaction mixture. Stirred sequentially at the same temperature under a nitrogen atmosphere for 2 d, the mixture was then dialyzed in DMF and deionized water using dialysis membranes (a molecular weight cut-off of 2 kDa) for 12 h. Next, the dialysate was filtered through a microfiltration membrane (0.45 μm), and a dark red solid was obtained after freeze-drying (80% yield).

Synthesis of 3, 3′-diselane diyldipropionic acid (DSeDPA)

Referring to a previous literature [26], selenium powder (1.825 g, 15 mmol) was mixed with 5 mL deionized water in a flask under a nitrogen atmosphere to form a black suspension. Then, $NaBH_4$ (1.135 g, 30 mmol) was dissolved in 12.5 mL deionized water and slowly added to the suspension in ice water. The reaction mixture was stirred at 0℃ for an hour until it became colorless and transparent. Next, the same amount of selenium powder (1.825 g, 15 mmol) was introduced and the mixture was continuously stirred at 105℃ for 30 min when the solution turned brown. After the pH value of the brown solution was adjusted to 8 with sodium carbonate, a solution of 3-bromopropionic acid (4.59 g, 30 mmol) in 7.5 mL deionized water was added. The reaction was maintained at room temperature for 12 h under the protection of nitrogen. The resulting solution was filtered and acidified with 1 mol/L HCl solution. Followed by extraction twice with ethyl acetate (EA), the precipitates were dried under vacuum. A yellow powder was obtained by recrystallization twice from EA (58% yield).

Synthesis of HOOC-SeSe-Cur-PEG-Cur-SeSe-COOH (PEG-Cur-SeSe-COOH)

A mixture of DSeDPA (2.29 g, 7.49 mmol) with acetic anhydride (15 mL) was stirred at 40℃ under a nitrogen atmosphere overnight. Toluene (10 mL) was then poured into the mixture, and the solvent was removed under vacuum. This process was repeated twice until the acetic anhydride was completely removed. The residue was subsequently dissolved in DCM (15 mL) with PEG-Cur (3.62 g, 1.25 mmol) and DMAP as the catalysts. The mixture was stirred at room temperature under a nitrogen atmosphere for a day and dialyzed in deionized water. The dialysate was filtered through a microfiltration membrane and the filtrate was freeze-dried to produce an orange solid (77% yield).

Synthesis of HOOC-SeSe-Cur-PEG-Cur-SeSe-PCL (PEG-Cur-SeSe-PCL)

Similarly, PEG-Cur-SeSe-COOH (4.03 g, 1.16 mmol) was dissolved in DMF (15 mL) followed by adding EDCI (0.67 g, 3.48 mmol), HOBt (0.47 g, 3.48 mmol), and PCL (2.32 g, 1.16 mmol). Under a nitrogen atmosphere, the reaction solution was stirred at room temperature for 24 h and dialyzed in DMF and deionized water for 12 h. A yellow product was finally obtained by the filtration through a microfiltration membrane and freeze-drying (68% yield).

Characterization of the polymer and its intermediates

The amphiphilic polymer PEG-Cur-SeSe-PCL and the intermediates during the synthesis were characterized by nuclear magnetic resonance (^{1}H-NMR, 400 MHz, Bruker, Germany) and fourier-transform infrared spectroscopy (FTIR, Nicolet IS50, Thermo Fisher Scientific, Massachusetts, USA). ^{1}H-NMR spectra were collected after the samples were dissolved in $CDCl_3$. FTIR measurement (500-4000 cm^{-1}) was performed at room temperature using KBr pellet. Differential scanning calorimetry (DSC 6000, PerkinElmer, USA) was employed to determine the thermomechanical properties of various polymers in the temperature range of 25-200 ℃ under a nitrogen atmosphere for 17.5 min.

Preparation of WR-1065-loaded NPs

WR-1065-loaded NPs were fabricated using an improved double emulsion-solvent evaporation technique (W/O/W) [27, 28]. First, the internal water phase (W_1 phase) was prepared by dissolving WR-1065 (120 mg) in 0.2 mL deionized water using ultrasound. The organic phase containing the polymer PEG-Cur-SeSe-PCL (100 mg) in DCM (2 mL) was emulsified with the W_1 phase by ultrasound (150 W) for one minute in an ice-water bath to form the primary emulsion (W_1/O). 7 mL deionized water as the external water phase (W_2 phase) was added to the above emulsion and emulsified by ultrasound (150 W) for a minute to form the multiple emulsions (W_1/O/W_2). Next, the organic solvent in the multiple emulsion was removed under vacuum, and the obtained residue was filtered through a microfiltration membrane to generate a colloidal solution of WR-1065-loaded NPs. Finally, these fresh NPs were dialyzed in deionized water for 24 h before being sealed and stored at 4 ℃ for future usage.

Characterization of NPs

The standard curve of WR-1065 was confirmed using high-performance liquid chromatography (HPLC, 1260 Infinity Agilent Technologies, USA). WR-1065 (100 mg) was dissolved in deionized water (10 mL) and then diluted into solutions of different concentrations (2 mg/mL, 4 mg/mL, 5 mg/mL, 6 mg/mL, and 8 mg/ml). The individual solution (5 μL) was pumped into an Inertsil ODS-SP C18 column (250 mm × 4.6 mm, 5 μm) at a flow rate of 0.7 mL/min at 30℃. Mobile phase A was methanol and mobile phase B was an aqueous solution of sodium 1-heptanesulfonate (3.5 mmol/L, adjusted to pH 7 with phosphoric acid). Phases A and B were both maintained at a concentration of 50% for 7 min. UV absorption intensity of WR-1065 was recorded at 220 nm. According to correlation between the peak area and corresponding concentration, the standard curve of WR-1065 was plotted.

The NPs (0.5 mL) loaded with WR-1065 were diluted with deionized water (0.5 mL), and the obtained solution (0.5 μL) was pumped into the uniform column at a flow rate of 0.7 mL/min at 30℃. Phase A was gradually increased from 10 to 50% within 5 min, while phase B was decreased from 90 to 50% at the same time; subsequently, phases A and B were maintained at a concentration of 50% for 10 min. With the assistance of the standard curve of WR-1065, the drug loading capacity (DLC) and drug loading efficiency (DLE) were calculated according to the following formula:

$$DLC\,(\%) = \frac{weight\ of\ WR?1065\ in\ NPs}{weight\ of\ NPs} \times 100\% \quad (1)$$

$$DLE\,(\%) = \frac{weight\,of\,WR?1065\,in\,NPs}{weight\,of\,WR?1065\,added\,to\,NPs} \times\,100\% \quad (2)$$

WR-1065-loaded NPs were dispersed in deionized water. Then, a laser particle size analyzer (LPSA, BI-200SM, Brookhaven Instruments, USA) was used to measure the average diameter and size distribution at room temperature. At least three measurements were conducted to obtain an average value. The morphology of the NPs was observed using high-resolution field-emission transmission electron microscopy (TEM, FEI-Tecnai G2 Spirit TWIN, USA). A few drops of the NPs were air-dried on a copper grid at room temperature before TEM analysis was performed on a chosen area of the sample.

Stability of NPs in the imitative gastric environment

Imitative gastric juice was prepared as follows. Hydrochloric acid (3.64 mL) was diluted in deionized water (10 mL). Deionized water (80 mL) and pepsin were sequentially added to a flask containing the diluted hydrochloric acid solution (1.64 mL). Water was then added to make the total volume to 100 mL. After transitory oscillation, artificial gastric juice was obtained (pH 1.2).

The drug-loaded NPs and free WR-1065 powder were transferred into the gastric juice placing on a shaker at 37℃, which mimicked the gastric environment of humans. At specified time intervals (0, 1, 2, 3, 4, and 6 h), a definite volume of the mixture (1 mL) was taken to determine the remaining concentration of WR-1065 by HPLC.

ROS-sensitive degradation of NPs in vitro

Fenton's reagent was prepared as follows. An aqueous solution of hydrogen peroxide (30% H_2O_2, 2 mL) was diluted to 20 mL by deionized water. Then, ferrous sulfate powder was added to the above solution in batches, and the obtained suspension was stirred for more than 10 min, resulting in the production of Fenton's reagent (3% $H_2O_2/FeSO_4 = 4:1$).

The NPs (2 mL) were added to freshly-prepared Fenton's reagent (10 mL) and the mixture was stirred at room temperature. The suspension (2 mL) was collected at preset intervals (1 and 2 h) and then extracted with DCM. The organic phase was dried over anhydrous sodium sulfate and subsequently removed under a reduced pressure. The obtained residue was characterized by ^{1}H-NMR spectroscopy. After the remnant suspension was left standing for 30 min, the supernatant was taken to observe the size and morphology of NPs under ROS conditions using LPSA and TEM.

30-day survival rate

Forty male C57BL/6J mice (23-24 g) were divided into the following five groups ($n = 8$) at random: (i) control, (ii) IR, (iii) IR + WR-1065 (150 mg/kg), (iv) IR + WR-1065-loaded NPs (350 mg/kg, containing 150 mg/kg WR-1065 and 15 mg/kg curcumin), and (v) IR + blank NPs (350 mg/kg). Mice in group iii-v were orally administered the corresponding drugs an hour prior to irradiation. Total body irradiation (8 Gy) was applied to mice at a rate of 0.99 Gy/min using a ^{137}Cs γ-ray irradiator (Atomic Energy of Canada Ltd., Ontario, Canada). The survival of the mice was recorded for 30 days to determine the initial radioprotective effect of the NPs.

Histological analysis

Twenty male C57BL/6J mice were randomly assigned to four groups ($n = 5$): (i) control, (ii) IR, (iii) IR + WR-1065 (150 mg/kg), and (iv) IR + WR-1065-loaded NPs (350 mg/kg). After the oral administration of drugs for 1 h, the abdomen of mice received 15 Gy γ rays at a rate of 0.99 Gy/min and the other parts were shielded by a lead block. On the 7th day after irradiation, each mouse was sacrificed, and their small intestines were collected. One part of the intestinal tissue was fixed in a 10% neutral buffered formalin solution, dehydrated, and embedded into paraffin blocks, while another part was stored at -80℃ for subsequent experiments. These blocks were evenly cut into 3 μm-thick sections, then deparaffinized, rehydrated, and stained with hematoxylin and eosin (H&E). Histological images were acquired using a microscope (Olympus, Tokyo, Japan) to observe acute damage and restoration of the small intestines.

Immunohistochemical analysis

The deparaffinized and rehydrated intestinal sections were incubated in 3% H_2O_2 solution for 15 min at 37℃ to remove the endogenous peroxidases, boiled in the citrate buffer solution, and then blocked with normal goat serum. The washed sections were incubated with the following primary antibodies: anti-Olfactomedin 4 (Olfm4) (1:200 dilution, CST), anti-Lysozyme (1:1000 dilution, Abcam), anti-Ki67 (1:200 dilution, CST), anti-γ-H2AX (1:5000 dilution, Abcam), anti-Caspase-3 (1:1000 dilution, Abcam), and anti-Caspase-9 antibody (1:300 dilution, Abcam) overnight at 4℃. Next, the sections were incubated with appropriate secondary antibodies for an hour at 37℃. Eventually, the sections were stained with hematoxylin after adding the DAB kit. Immunohistochemical images were acquired using a microscope and the stained areas were analyzed by ImageJ software (USA).

Statistical analysis

The Kaplan-Meier method and log-rank test were adopted to analyze the 30-day survival rate in different groups, and an unpaired t-test (two-tailed) was applied to evaluate the discrepancy between groups. The data

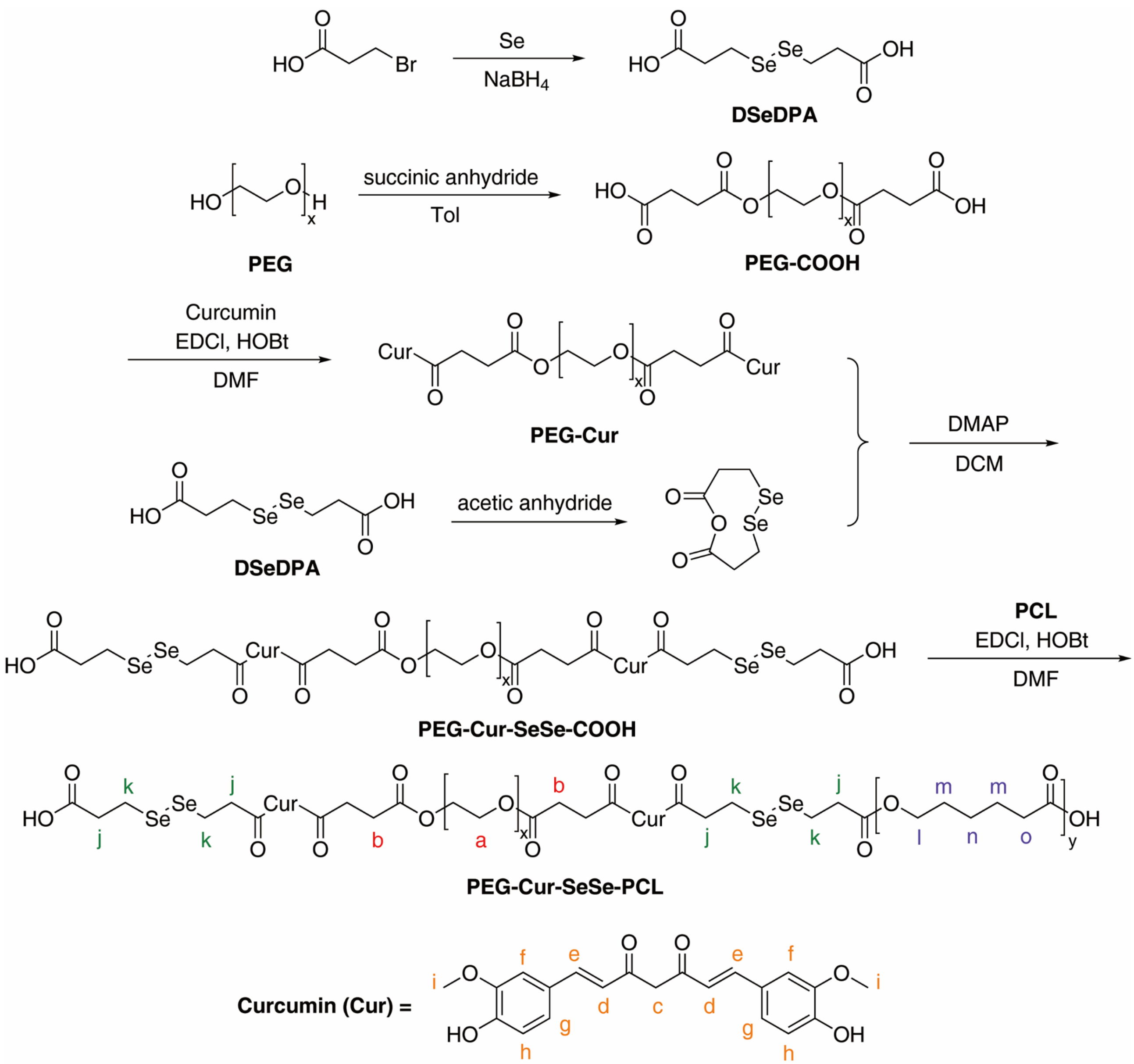

Fig. 1 Synthetic route of the polymer PEG-Cur-SeSe-PCL (Hydrogen atoms located in different positions of the polymer and curcumin are labeled with different letters)

are presented as the mean ± SEM and the significant differences were set at $p < 0.05$. All experimental data were analyzed using Origin 8 (Massachusetts, USA) and GraphPad Prism 9.0 (California, USA).

Results

Preparation and characterization of the polymers

The fabrication of a ROS-responsive amphiphilic polymer linked by curcumin, PEG-Cur-SeSe-PCL, was successfully completed through a series of four esterification reactions (Fig. 1). First, the raw material PEG-2000 was subjected to a condensation reaction with succinic anhydride, resulting in the formation of PEG-COOH. Curcumin, known for its two symmetric phenolic hydroxyl groups, was then utilized as a bridging molecule and engaged in two condensations with PEG-COOH and DSeDPA, respectively. Following the above reactions, the final step involved the conjugation of the the carboxyl group in DSeDPA with the hydroxyl group in PCL-2000, resulting in the formation of the desired amphiphilic polymer, PEG-Cur-SeSe-PCL.

The ^{1}H-NMR spectroscopy was employed to characterize the polymer PEG-Cur-SeSe-PCL and its intermediates, with the results illustrated in Fig. 2A. The peak at 3.6 ppm (a) was identified as the methylene unit of PEG, while the peak at 2.7 ppm (b) corresponded to

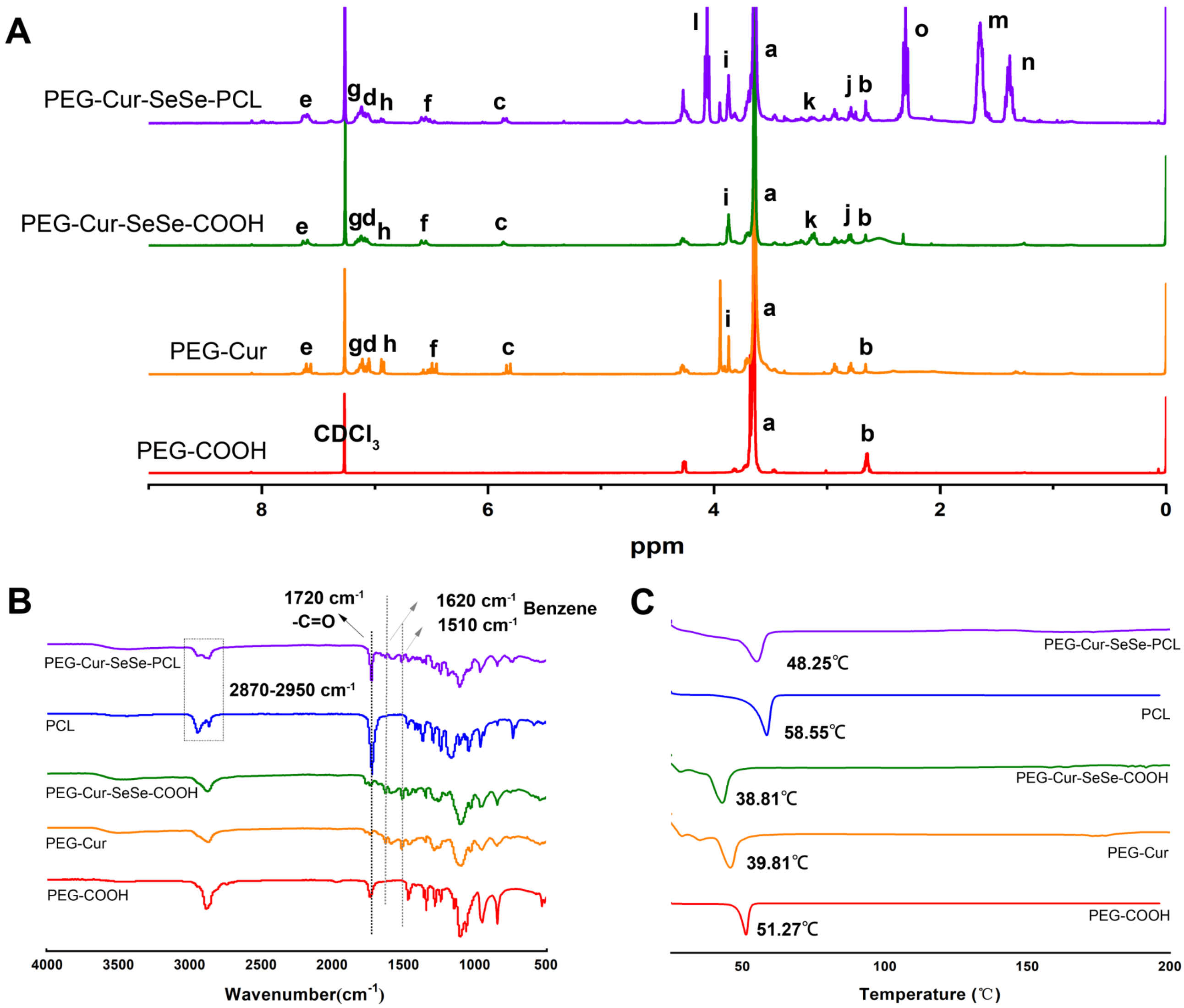

Fig. 2 Characterization of PEG-Cur-SeSe-PCL and its intermediates. (**A**) ^{1}H-NMR spectrum (400 MHz, $CDCl_3$). (**B**) FTIR spectra (500-4000 cm^{-1}). (**C**) DSC curves showing the melting temperature (0-200℃)

the methylene of succinic anhydride. The peaks ranging from 7.6 to 5.8 ppm (c-h) were attributed to various hydrogen atoms on the unsaturated carbon in curcumin and the hydrogens on the methoxy moiety was found at 3.9 ppm (i). The spectrum also demonstrated that the peaks at approximately 3.1 ppm (j) and 2.7 ppm (k) were associated with the two distinct methylene groups from DSeDPA, accompanied by several peaks (l-o) corresponding to the methylene protons in PCL. By comparing the integrated peak areas assigned to the phenyl hydrogens of curcumin (approximately 6.9 ppm, h) and methylene protons (3.6 ppm, a) of PEG, the content of conjugated curcumin in PEG-Cur-SeSe-PCL was calculated as 10.1 weight% (wt%). This calculation suggests a molar ratio of PEG to curcumin of approximately 1:1.5. Similarly, the molar ratio of PEG to PCL in the polymer was deduced to be about 1:1.

As depicted in Fig. 2B, the chemical structure of PEG-Cur-SeSe-PCL was verified using FTIR spectroscopy. Compared with PEG-COOH and PCL, two distinctive absorption peaks at 1510 cm^{-1} and 1620 cm^{-1} were assigned to the C = C stretching of benzene, confirming the conjugation of curcumin to the polymer backbone. Moreover, the combination of PEG-Cur-SeSe-COOH and PCL was evidenced by changes in the absorption peaks at 2870-2950 cm^{-1} (C-H stretching vibrations of alkane groups) and the sharp peak at 1720 cm^{-1} (carbonyl group stretching). Fig. 2C illustrates the variation in the melting temperature of the polymers at each synthetic step, which provides further support for the successful synthesis of PEG-Cur-SeSe-PCL.

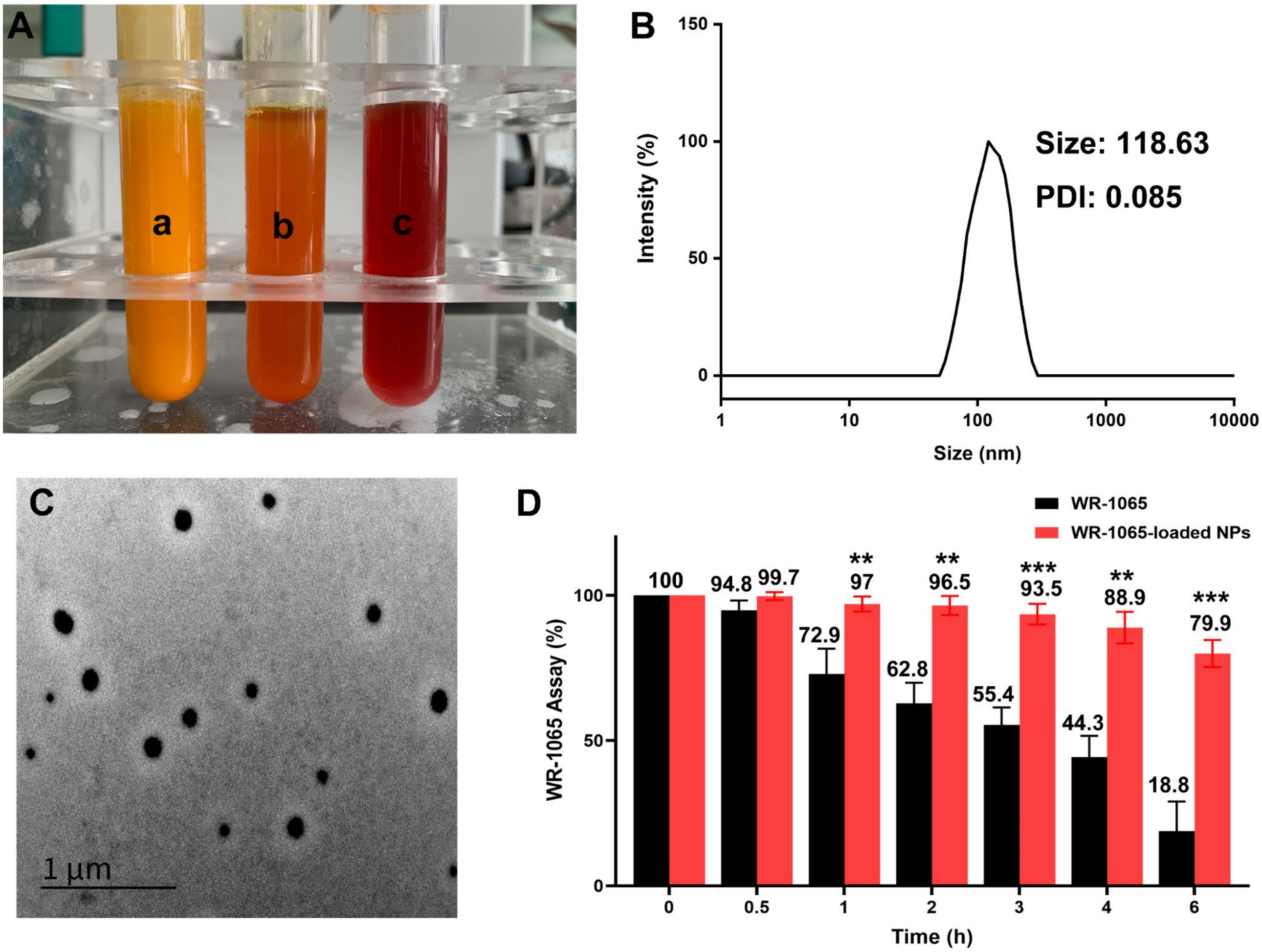

Fig. 3 Characterization of NPs. (**A**) The image showing the solubility of curcumin (**a**), polymer (**b**), and NPs (**c**) in deionized water. The equivalent weight of curcumin was 10 mg/ml. (**B**) LPSA results with an average diameter and PDI. (**C**) Particle morphology of NPs by TEM (Scale bar: 1 µm). (**D**) The comparison in the stability of WR-1065 and WR-1065-loaded NPs in gastric juice (pH 1.2) for 6 h. The data were shown as mean ± SEM ($n = 3$). WR-1065 *vs.* WR-1065-loaded NPs, $^{**}p < 0.01$ and $^{***}p < 0.001$

Preparation and characterization of NPs

WR-1065-loaded NPs were prepared using the double emulsion-solvent evaporation technique. As observed in Fig. 3A, free curcumin (a) showed poor solubility in water, while both the polymer PEG-Cur-SeSe-PCL (b) and the NPs produced from the polymer (c) demonstrated excellent water solubility, suggesting that these particles have the potential to enhance the bioavailability of curcumin in vivo.

Utilizing the standard curve of WR-1065, the DLC and DLE of the NPs were determined to be 30.9% and 56.7%, respectively (Supplementary Table 1-2). The values indicate that this nanocarrier addressed the common issue of low drug loading in traditional formulations. Fig. 3B presents data showing that the mean diameter of the NPs was 118.63 nm, with a polydispersity index (PDI) of 0.085. Moreover, the TEM image in Fig. 3C revealed that the particles were spherical in shape and dispersed uniformly. This observation is consistent with the results from the LPSA, confirming the successful fabrication of well-defined NPs.

Stability of NPs in the imitative gastric environment

The stability of free WR-1065 and the NPs loaded with WR-1065 in a simulated human gastric environment was evaluated (Fig. 3D; Supplementary Table 3). In the imitative gastric environment, the content of free WR-1065 experienced a significant reduction, with almost 81% degradation observed over a period of 6 h. In stark contrast, WR-1065 encapsulated in NPs demonstrated significantly enhanced stability. Over the same 6-hour period, there was only a 20% decrease in the content of WR-1065 when it was loaded onto the NPs. This result suggests that the NPs provide a protective environment for WR-1065, significantly reducing its metabolic rate in the gastric juice.

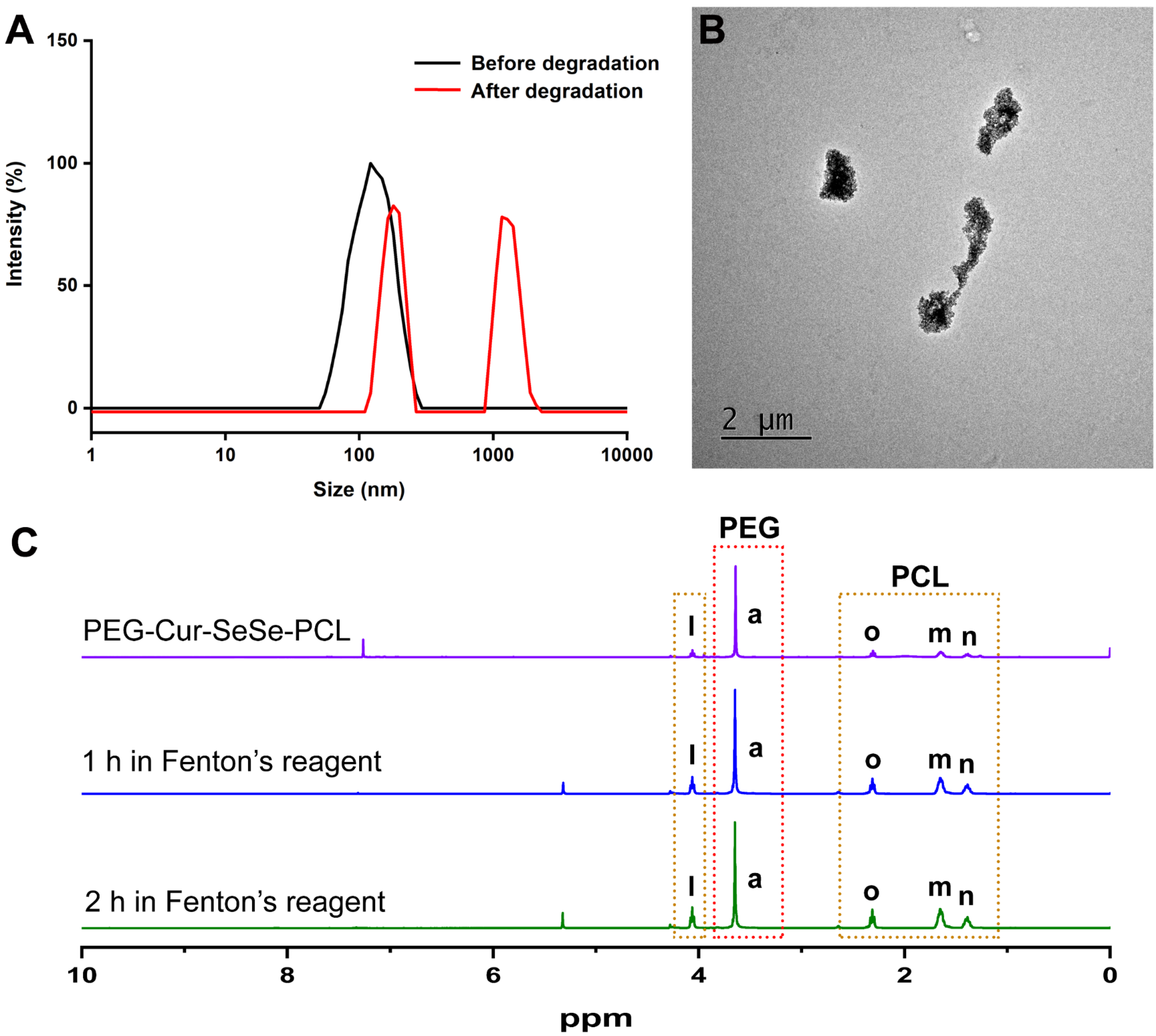

Fig. 4 ROS-sensitive property of NPs. (**A**) The alteration in the size of NPs before and after degradation with the Fenton's reagent. (**B**) The TEM image of NPs with Fenton's reagent (Scale bar: 2 μm). (**C**) ^{1}H-NMR spectra showing the radio of PCL (**l-o**) to PEG (**a**) before and after degradation with the Fenton's reagent in 1 and 2 h

ROS-sensitive degradation of NPs in vitro

The degradation behavior of the NPs in response to ROS was assessed using a Fenton's reagent (3% H_2O_2/$FeSO_4$ = 4:1). As evidenced by LPSA results shown in Fig. 4A, the size of these particles increased upon the addition of Fenton's reagent. The TEM image provided in Fig. 4B, taken after the degradation process, shows a contrast to the initial state depicted in Fig. 3C. The NPs, which were initially spherical and uniformly dispersed, aggregated to form large and irregularly shaped structures. Additionally, a significant increase in the ratio of methylene groups of PCL (l-o) to PEG (a) in the ^{1}H-NMR spectra was observed after the NPs were exposed to the Fenton's reagent for 2 h (Fig. 4C). The observed degradation behavior of NPs suggests that they were able to be exploited to trigger the release of drugs including WR-1065 in the presence of ROS.

NPs improved the survival rate of irradiated mice

To evaluate the preliminary radioprotective effect of WR-1065-loaded NPs, a 30-day survival study on mice subjected to different treatment was conducted. The results in Fig. 5 show that all mice receiving not treatment (group i) remained alive throughout the one-month observation period, while the survival rate of mice only receiving irradiation of 8 Gy (group ii) dropped to 50% by day 16. By day 24, none of mice in group ii survived. When mice were given WR-1065 orally before irradiation

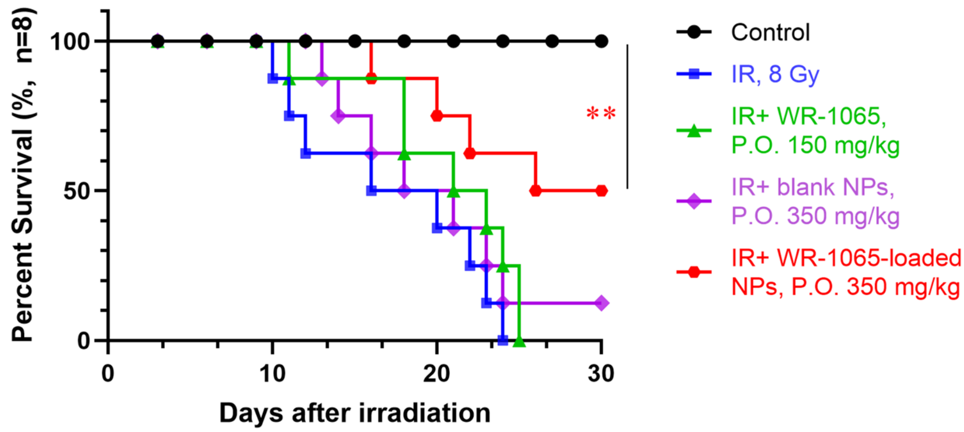

Fig. 5 The 30-day survival rate of mice after whole-body irradiation of 8 Gy ($n=8$). **$p<0.01$

(group iii), there was an initial improvement in the survival rate compared to group ii, with a higher percentage of mice surviving up to day 24 or 25. However, the survival rate eventually in group iii dropped to 0%. Mice pre-treated with WR-1065-loaded NPs (group iv) demonstrated a statistically significant improvement in survival rate, with 50% of the mice surviving up to the 30th day ($p=0.0062$). Even the blank NPs without WR-1065 showed a slight improvement in the survival rate (up to 12.5%), which attributed to the ROS scavenging capacity of curcumin and Se-Se bonds present in the NPs.

NPs alleviated radiation-induced damage to the small intestine

The 30-day survival rate results demonstrated that WR-1065-loaded NPs had a radioprotective effect on the irradiated mice. To delve deeper into this protective effect, especially on the small intestine which is highly sensitive to IR, a histological analysis was carried out. As shown in Fig. 6A, the structure of crypt cells was severely compromised and intestinal villi were shortened after irradiation in the mice receiving only irradiation (group ii), underscoring the destructive impact of IR on the intestine of mice. In contrast, mice that were administered WR-1065-loaded NPs (group iv) before irradiation showed a marked improvement in intestinal structure. The destruction of crypt cells and villi was considerably mitigated compared to group ii, suggesting that the integrity of the epithelial structure in the small intestine was maintained. Comparatively, mice that were given pure WR-1065 orally (group iii) did not show the same degree of intestinal recovery and protection as those treated with the NPs.

NPs improved the proliferative and regenerative ability of irradiated intestine stem cells (ISCs)

This study aimed to assess the impact of NPs on the ISCs capacity for proliferation and regeneration by examining the expression of Ki67, Olfm4 and Lysozyme using immunohistochemical methods. Fig. 6B-C shows that there is an evident reduction in the expression of Olfm4 and Ki67 after irradiation in comparison with the control group. The quantity of these two markers were increased markedly when pre-treated with WR-1065-loaded NPs (Fig. 6E-F; Olfm4, $p<0.001$; Ki67, $p<0.05$). This increase was not observed in mice treated with WR-1065 alone, highlighting the enhanced effectiveness of NPs in promoting ISCs regeneration. As depicted in Fig. 6D and G, the expression of Lysozyme was adversely affected by irradiation. However, NPs prominently improved the positive expression of Lysozyme ($p<0.01$) while there was no obvious change with the administration of WR-1065 alone, indicating that NPs reversed the impairment of Paneth cells with the increased secretion of Lysozyme.

NPs alleviated radiation-induced damage to the small intestine via reducing DNA damage and apoptosis

To assess the impact of NPs on DNA damage within the intestine of irradiated mice, we conducted an immunohistochemical analysis focusing on the expression of γ-H2AX, a well-established marker of double-strand breaks (DSBs) [29]. Our results, depicted in Fig. 7A and D, reveal an increase in γ-H2AX expression in irradiated mice compared to the control group, indicative of heightened DNA damage. Notably, the oral administration of WR-1065-loaded NPs significantly lowered the expression of γ-H2AX ($p<0.05$), suggesting a protective effect against radiation-induced DNA impairment.

Further investigation into the protective mechanism of NPs on the small intestine involved examining apoptosis, a process triggered by DNA damage [30]. Caspase-9 and -3 were chosen as the key markers to explore this aspect. As illustrated in Fig. 7B-C and E-F, the expression of both Caspase-9 and -3 was elevated in mice following partial irradiation. However, pre-treatment with WR-1065-loaded NPs in advance reduced the levels of

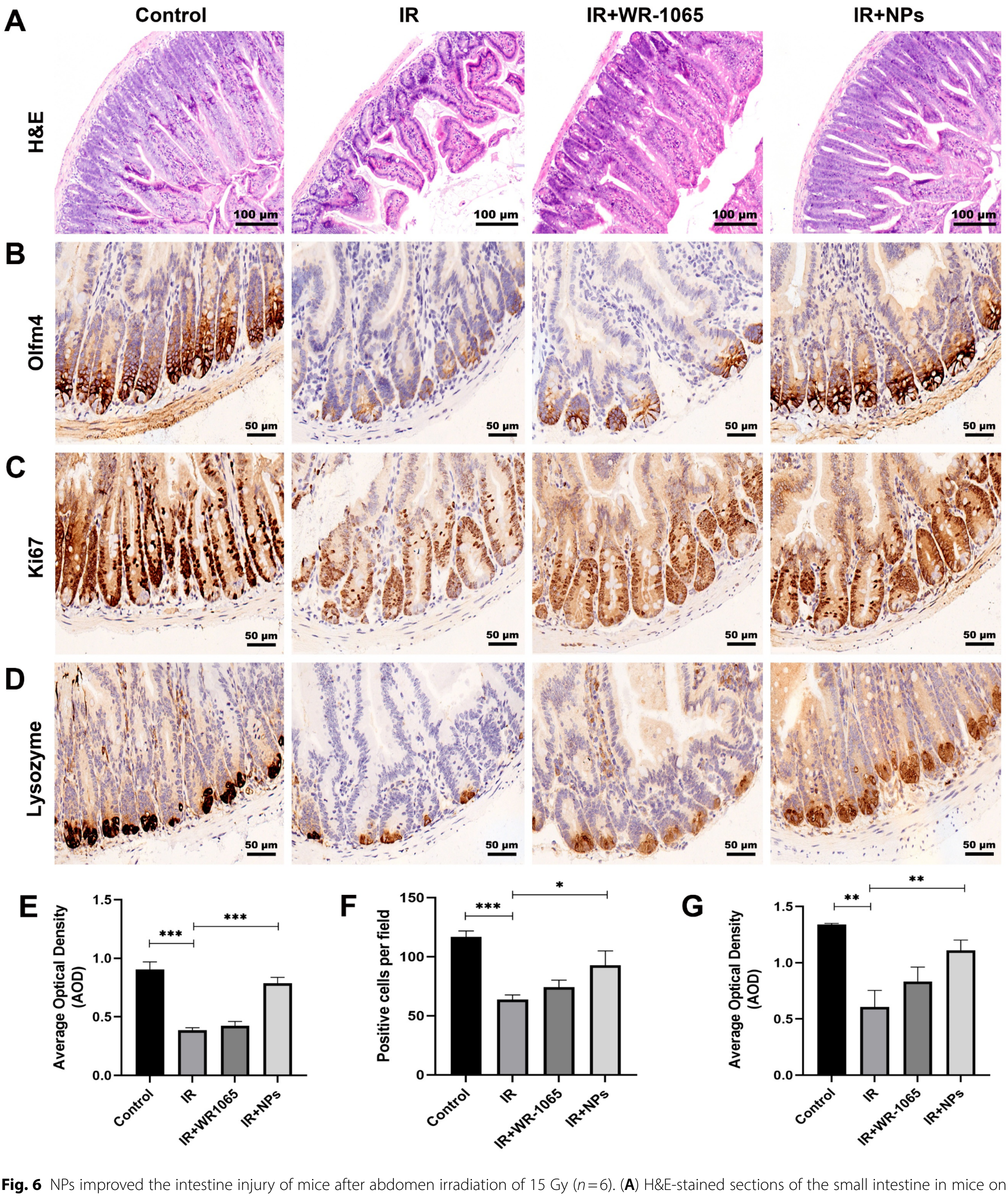

Fig. 6 NPs improved the intestine injury of mice after abdomen irradiation of 15 Gy (n = 6). (**A**) H&E-stained sections of the small intestine in mice on the 7th day after irradiation (Scale bar: 100 μm). (**B**-**D**) Immunohistochemistry images on the expression of Olfm4 (**B**), Ki67 (**C**), and Lysozyme (**D**) in the sections of mice on the 7th day after irradiation (Scale bar: 50 μm). (**E**-**G**) Quantitative analysis of these three markers including Olfm4 (**E**), Ki67 (**F**), and Lysozyme (**G**). The data were shown as mean ± SEM (n = 3). *p < 0.05, **p < 0.01, and ***p < 0.001

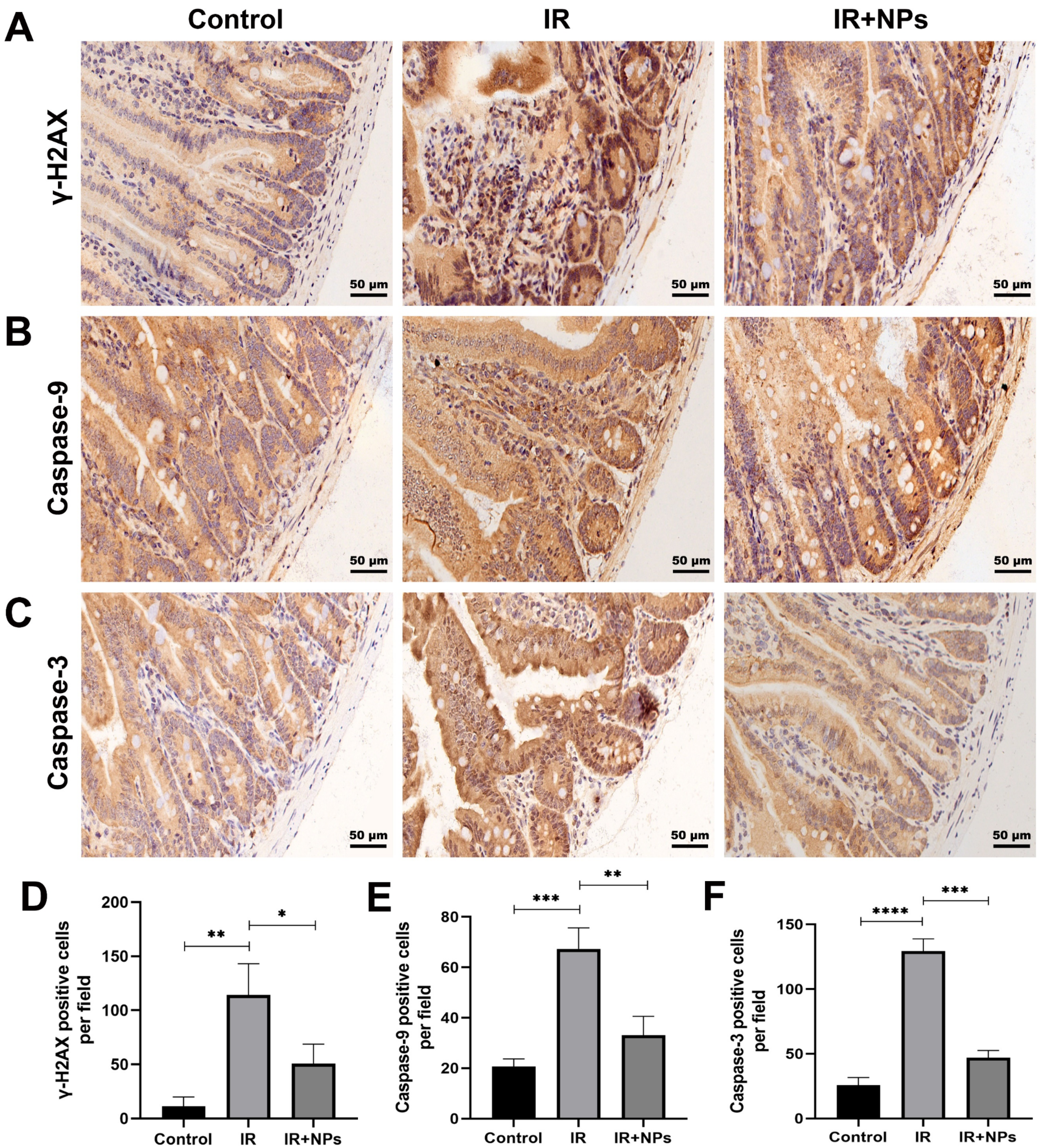

Fig. 7 NPs reduced DNA damage and inhibited apoptosis of the small intestine ($n = 6$). (**A**-**C**) Immunohistochemistry images on the expression of γ-H2AX (**A**), Caspase-9 (**B**) and -3 (**C**) in the sections of mice on the 7th day after irradiation (Scale bar: 50 μm). (**D**-**F**) Statistical results of markers including γ-H2AX (**D**), Caspase-9 (**E**) and -3 (**F**). The data were shown as mean ± SEM ($n = 3$). *$p < 0.05$, **$p < 0.01$, ***$p < 0.001$, and ****$p < 0.0001$

Caspase-9 ($p < 0.01$) and -3 ($p < 0.001$). These findings indicate that NPs may exert their radioprotective effect, in part, by inhibiting the apoptotic pathway triggered by IR.

Discussion

In recent advancements, a variety of DDS including nanomaterials [31, 32], hydrogels [33], microalga [34], and microspheres [35], have been crafted to facilitate the oral administration of amifostine or WR-1065, offering patients a more convenient therapeutic approach. The swift progression of nanotechnology has given rise to nanomaterials-based delivery platforms using poly (lactide-co-glycolide) (PLGA) [31], PEG/PCL [33, 36], and metal-organic frameworks (MOFs) [37], which address the inherent shortcoming of drugs, bolster the radioprotective efficacy, and alleviate acute radiation-induced damage. In this paper, we successfully synthesized a novel curcumin-containing amphiphilic polymer embedded with Se-Se bonds as ROS-sensitive groups (PEG-Cur-SeSe-PCL, Fig. 1). The polymer was assembled to spherical NPs loaded with WR-1065 (WR-1065-loaded NPs) via the double emulsion-solvent evaporation, showcasing high loading capacity and efficacy. According to the preparation procedure, WR-1065 was encapsulated in the hydrophilic core of the amphiphilic NPs while curcumin was situated in the hydrophobic layer.

As a thiol compound, WR-1065 is susceptible to oxidation reactions under the acidic conditions, leading to the formation of disulfides (WR-33278) [38, 39]. Our findings indicated that WR-1065 exhibited poor stability in simulated gastric juice (Fig. 3D). Previous studies have established that the radioprotective effect of amifostine on normal cells is primarily correlated with its thiol form (WR-1065), rather than WR-33278 [40]. As previously reported [41], the PEG/PCL-based NPs were effective in maintaining the stability of WR-1065 in the same environment (Fig. 3D), suggesting that NPs protected WR-1065 from fast metabolization in the gastric environment.

The low oral bioavailability of curcumin is primarily attributed to its poor intestinal absorption, related to both low water solubility and chemical instability, as well as hepatic reduction and conjugation metabolism [42]. The therapeutic potential of curcumin remains controversial, even when administered at high dosage (12 g/day) [43]. To address this pharmacological challenge, advanced DDS such as amphiphilic polymer-based NPs, have emerged as effective solutions [44, 45]. For instance, PEG/PCL-based NPs loaded with curcumin showed a 3.18-fold increase in the area under the concentration-time curve (AUC, an index for evaluating bioavailability) with the mean residence time (MRT) extending from 0.169 to 40.148 h [46]. Similarly, linolenic acid (LNA)-modified PEG/PCL micelles increased curcumin's solubility to 2.05 mg/mL in water, which was approximately 1.87×10^5 times higher than that of free curcumin. Furthermore, the AUC and MRT of micelles in the plasma were 2.75- and 3.49-fold higher than that of control solution, respectively [47]. In our study, both the polymer PEG-Cur-SeSe-PCL (b) and the NPs produced from the polymer (c) demonstrated improved water solubility (Fig. 3A), further validating the potential of WR-1065-loaded NPs to improve curcumin's bioavailability.

In the absence of ROS, the polymer degradation was slow, releasing curcumin primarily through the hydrolysis of ester bonds in the polymer [48]. When exposed to ROS, the redox-sensitive Se-Se bonds in the amphiphilic polymer underwent oxidation and cleavage [23], accelerating the release of WR-1065 and curcumin. *Miao et al.* proposed that NPs degraded in the presence of ROS contributed to the aggregation of hydrophobic segments in the polymer with the increased methylene ratio of PCL to PEG [36], which was consistent with our results (Fig. 4C). Additionally, PEG/PCL-based NPs have been reported to rapidly accumulate in the intestinal tract within 0.5 h post-administration and persist for up to 4 h [41]. It hinted that more WR-1065 and curcumin were delivered by these ROS-sensitive NPs to the small intestine where excessive ROS was available, thereby jointly exerting the radiation protection effect.

The 30-day survival rate of mice subjected to a lethal exposure dose (8 Gy), serves as a crucial index to evaluate the efficacy of radioprotective agents [49]. As shown in Fig. 5, the death time of mice in group iii postponed, implying that WR-1065 provided some protection on the irradiated mice but the protective effect was suppressed over time due to the instability and poor oral bioavailability of WR-1065 in vivo. Oral administration of WR-1065-loaded NPs (group iv) prominently improved the survival rate, which suggested NPs enhanced the radioprotective effect of WR-1065 on the irradiated mice. The small intestine, being highly sensitive to radiation [36], experiences acute injury exposed to a high dose of IR characterized by apoptosis-induced destruction of crypt cells, reduction in the length and number of villi, and compromise of the epithelial barrier, contributing to the subsequent inflammatory infiltration [50, 51]. Our histological results in Fig. 6A demonstrated that the local abdominal irradiation caused less morphological damage in the intestine of mice in group iv compared with group ii, suggesting that NPs amplified the potential synergistic radiation protection of WR-1065 and curcumin.

ISCs are pivotal in maintaining the intestinal homeostasis and instrumental in the epithelial regeneration following radiation [52]. The protein Olfm4 is one of the identified markers for active ISCs (aISCs), which are sensitive to IR owing to their rapid multiplication rate [53]. Ki67 is also a vital index for gauging the proliferation and regeneration of ISCs [54]. Exposure to high doses of IR depletes the population of ISCs and obstructs epithelial renewal, which consequently impairs mucosal integrity and creates a vulnerability to bacterial pathogens [55]. Specialized intestinal epithelial cells, Paneth cells, play a defensive role to counteract these pathogens through secreting antimicrobial substances such as Lysozyme [51]. As presented in Fig. 6B-G, the improved integrity of the epithelial structure in group iv was probably due to the reduction in the great loss of ISCs caused by IR and the enhancement in the proliferative function of ISCs, suggesting that WR-1065-loaded NPs increased the survival of aISCs and supported the maintenance of epithelial renewal.

Systemic or partial exposure to a high-dose IR can directly or indirectly damage the most important target DNA molecules through base damage, single-strand breaks (SSBs), and DSBs [56]. DSBs are especially detrimental as they can severely disrupt cell viability, potentially initiating cell death through apoptosis or inducing cellular senescence [8]. The rupture of mitochondrial permeability can be triggered by DNA damage, resulting in the release of apoptotic factor cytochrome c [57]. The combination of the apoptotic peptidase activating factor 1 (Apaf-1) complex and dissociative cytochrome c, activating Caspase-9, -3 and -7, forms apoptosome and leads to intrinsic apoptosis [58]. Our immunohistochemical results indicated that NPs loaded with WR-1065 preferably alleviated DNA damage induced by γ-ray and inhibited apoptotic signaling pathway to protect the small intestine of mice (Fig. 7). In addition to this, more radioprotective mechanisms of WR-1065 have been reported, including the introduction of temporary cellular hypoxia through the Warburg-type effect [59], activation of nuclear transcription factor kappaB (NF-κB) [54], and enhanced expression of manganese superoxide dismutase (SOD2) [60]. Therefore, the radioprotective role of WR-1065 appears to be taken synergistically by multiple direct and indirect mechanisms.

Conclusion

In summary, these ROS-responsive NPs have demonstrated the ability to stabilize the metabolism of WR-1065, overcome the limitations of WR-1065's oral ineffectiveness, and enhance the radioprotective properties of WR-1065 particularly in the small intestine. The development of WR-1065-loaded NPs presents innovative strategies for the protection and treatment of ARI, offering promising potential in the field of radioprotection.

Abbreviations

IR	Ionizing radiation
ROS	Reactive oxygen species
PEG	Poly (ethylene glycol)
PCL	Polycaprolactone
NPs	Nanoparticles
ARS	Acute radiation syndrome
DDS	Drug delivery systems
$NaBH_4$	Sodium borohydride
HOBt	1-Hydroxybenzotriazole
DMAP	4-Dimethylaminopyridine
$FeSO_4$	Ferrous sulfate
EDCI	1-(3-Dimethylaminopropyl)-3-ethylcarbodiimide hydrochloride
H_2O_2	Hydrogen peroxide solution
IRM	Institute of Radiation Medicine
CAMS	Chinese Academy of Medical Sciences
DCM	Dichloromethane
DMF	Dimethylformamide
EA	Ethyl acetate
NMR	Nuclear magneticresonance
FTIR	Fourier-transform infrared spectroscopy
DSC	Differential scanning calorimetry
HPLC	High-performance liquid chromatography
DLC	Drug loading capacity
DLE	Drug loading efficiency
LPSA	Laser particle size analyzer
TEM	Transmission electron microscopy
H&E	Hematoxylin and eosin
Olfm4	Olfactomedin4
PDI	Polydispersity index
ISCs	Intestine stem cells
DSBs	Double-strand breaks
PLGA	Poly (lactide-co-glycolide)
MOFs	Metal-organic frameworks
aISCs	Active ISCs
SSBs	Single-strand breaks
Apaf-1	Apoptotic peptidase activating factor 1
NF-κB	Nuclear transcription factor kappaB
SOD2	Manganese superoxide dismutase
AUC	Area under the concentration-time curve
MRT	Mean residence time
LNA	Linolenic acid

Supplementary Information

The online version contains supplementary material available at https://doi.org/10.1186/s12951-025-03276-3.

Supplementary Material 1

Author contributions

Yichi Huang: Investigation, resources, methodology, data curation, writing-original draft, and writing-review & editing. Jiaze Li, Sen Wang: Resources and methodology. Hongqi Tian: Conceptualization, funding acquisition, and writing-review & editing. Saijun Fan: Project administration, supervision, and writing-review & editing. Yu Zhao: Supervision, validation, and writing-review & editing.

Funding

This work was supported in part by grants from the Non-profit Central Research Institute Fund of Chinese Academy of Medical Sciences (2021-RC310-010 to Y. Z.), the National Natural Science Foundation of China (81730086 to SJ. F.), the CAMS Innovation Fund for Medical Sciences (2021-I2M-1-042 to SJ. F.; 2021-I2M-1-060 to Y. Z.), the Tianjin Natural Science Foundation of Key Program (23JCZDJC00290 to Y. Z.), and the Science Foundation for Distinguished Young Scholars of Tianjin (24JCJQJC00080 to Y. Z.).

Data availability

The data and materials of this paper are fully original and available from the corresponding authors.

Declarations

Ethics approval and consent to participate

In accordance with the National Regulation of China for Care and Use of Laboratory Animal, the entire experiment was performed with the approval of the Animal Care and Ethics Committee of IRM, CAMS (SYXK 2024-0004).

Consent for publication

The manuscript has been approved to be published by all the authors.

Competing interests

The authors declare no competing interests.

Author details
[1]Tianjin Key Laboratory of Radiation Medicine and Molecular Nuclear Medicine, Institute of Radiation Medicine, Chinese Academy of Medical Sciences and Peking Union Medical College, Tianjin 300192, China
[2]Kechow Pharma, Inc., Shanghai 200131, China

Received: 19 August 2024 / Accepted: 24 February 2025
Published online: 22 March 2025

References

1. Tapio S, Little MP, Kaiser JC, Impens N, Hamada N, Georgakilas AG, Simar D, Salomaa S. Ionizing radiation-induced circulatory and metabolic diseases. Environ Int. 2021;146:106235.
2. Jahng JWS, Little MP, No HJ, Loo BW, Wu JC. Consequences of ionizing radiation exposure to the cardiovascular system. Nat Rev Cardiol. 2024;21:880.
3. Hou Y, Shang Y, Xu F, Li T, Li M, Wei L, Fan S, Hou W, Gou W, Shang H, Li Y. Ionizing radiation induces neurotoxicity in xenopuslaevis embryos through neuroactive ligand-receptor interaction pathway. Environ Res. 2024;256:119237.
4. Yadav M, Bhayana S, Liu J, Lu L, Huang J, Ma Y, Qamri Z, Mo X, Jacob DS, Parasa ST, Bhuiya N, Fadda P, Xu-Welliver M, Chakravarti A, Jacob NK. Two-miRNA-based finger-stick assay for Estimation of absorbed ionizing radiation dose. SciTransl Med. 2020;12:eaaw5831.
5. Kumagai T, Rahman F, Smith AM. The Microbiome and radiation induced-bowel injury: evidence for potential mechanistic role in disease pathogenesis. Nutrients. 2018;10:1405.
6. Tirado FR, Bhanja P, Castro-Nallar E, Olea XD, Salamanca C, Saha S. Radiation-induced toxicity in rectal epithelial stem cell contributes to acute radiation injury in rectum. Stem Cell Res Ther. 2021;12:63.
7. Li J, Wu DM, Yu Y, Deng SH, Liu T, Zhang T, He M, Zhao YY, Xu Y. Amifostine ameliorates induction of experimental autoimmune encephalomyelitis: effect on reactive oxygen species/NLRP3 pathway. IntImmunopharmacol. 2020;88:106998.
8. King M, Joseph S, Albert A, Thomas TV, Nittala MR, Woods WC, Vijayakumar S, Packianathan S. Use of amifostine for cytoprotection during radiation therapy: a review. Oncology. 2020;98:61.
9. Ji L, Cui P, Zhou S, Qiu L, Huang H, Wang C, Wang J. Advances of amifostine in radiation protection: administration and delivery. Mol Pharm. 2023;20:5383.
10. Wang C, Ji L, Wang J, Zhang J, Qiu L, Chen S, Ni X. Amifostine loaded lipid-calcium carbonate nanoparticles as an oral drug delivery system for radiation protection. Biomed Pharmacother. 2024;177:117029.
11. Hu X, Wong S-W, Liang K, Wu T-H, Wang S, Wang L, Liu J, Yamauchi M, Foster BL, Ting JPY, Zhao B, Tseng HC, Ko C-C. Optineurin regulates NRF2-mediated antioxidant response in a mouse model of Paget's disease of bone. Sci Adv. 2023;9:eade6998.
12. Akpolat M, Kanter M, Uzal MC. Protective effects of Curcumin against gamma radiation-induced ileal mucosal damage. Arch Toxicol. 2009;83:609.
13. Li Y, Cai Z, Ma W, Bai L, Luo E, Lin Y. A DNA tetrahedron-based ferroptosis-suppressing nanoparticle: superior delivery of Curcumin and alleviation of diabetic osteoporosis. Bone Res. 2024;12:14.
14. Amini P, Saffar H, Nourani MR, Motevaseli E, Najafi M, Ali Taheri R, Qazvini A. Curcumin mitigates radiation-induced lung pneumonitis and fibrosis in rats. Int J Mol Cell Med. 2018;7:212.
15. Shabeeb D, Musa AE, Abd Ali HS, Najafi M. Curcumin protects against radiotherapy-induced oxidative injury to the skin. Drug Des DevelTher. 2020;14:3159.
16. Chen Z, Farag MA, Zhong Z, Zhang C, Yang Y, Wang S, Wang Y. Multifaceted role of phyto-derived polyphenols in nanodrug delivery systems. Adv Drug Deliv Rev. 2021;176:113870.
17. Li R, Landfester K, Ferguson CTJ. Temperature- and pH-responsive polymeric photocatalysts for enhanced control and recovery. AngewChemInt Ed Engl. 2022;61:e202211132.
18. Wei D, Sun Y, Zhu H, Fu Q. Stimuli-responsive polymer-based nanosystems for cancer theranostics. ACS Nano. 2023;17:23223.
19. Cao Z, Zuo X, Liu X, Xu G, Yong K-T. Recent progress in stimuli-responsive polymeric micelles for targeted delivery of functional nanoparticles. Adv Colloid Interface Sci. 2024;330:103206.
20. Lei G, Zhang Y, Koppula P, Liu X, Zhang J, Lin SH, Ajani JA, Xiao Q, Liao Z, Wang H, Gan B. The role of ferroptosis in ionizing radiation-induced cell death and tumor suppression. Cell Res. 2020;30:146.
21. Han W, Zhang S, Qian J, Zhang J, Wang X, Xie Z, Xu B, Han Y, Tian W. Redox-responsive fluorescent nanoparticles based on diselenide-containing AIEgens for cell imaging and selective cancer therapy. Chem Asian J. 2019;14:1745.
22. Wei C, Liang B, Li Y, Yan B, Zhou Y, Liu Y, Lang. M. A drug-free therapeutic system for cancer therapy by diselenide-based polymers themselves. AdvHealthc Mater. 2021;10:e2001471.
23. Shao D, Li M, Wang Z, Zheng X, Lao Y-H, Chang Z, Zhang F, Lu M, Yue J, Hu H, Yan H, Chen L, Dong W-F, Leong KW. Bioinspired diselenide-bridged mesoporous silica nanoparticles for dual-responsive protein delivery. Adv Mater 2018: e1801198.
24. Hailemeskel BZ, Hsu W-H, Addisu KD, Andrgie AT, Chou H-Y, Lai J-Y, Tsai H-C. Diselenide linkage containing triblock copolymer nanoparticles based on Bi(methoxyl poly(ethylene glycol))-poly(ε-carprolactone): selective intracellular drug delivery in cancer cells. Mater SciEng C Mater Biol Appl. 2019;103:109803.
25. Li T, Pan S, Gao S, Xiang W, Sun C, Cao W, Xu H. Diselenide-pemetrexed assemblies for combined cancer immuno-, radio-, and chemotherapies. AngewChemInt Ed Engl. 2020;59:2700.
26. Sun B, Luo C, Zhang X, Guo M, Sun M, Yu H, Chen Q, Yang W, Wang M, Zuo S, Chen P, Kan Q, Zhang H, Wang Y, He Z, Sun J. Probing the impact of sulfur/selenium/carbon linkages on prodrug nanoassemblies for cancer therapy. Nat Commun. 2019;10:3211.
27. Xu B, Zhou W, Cheng L, Zhou Y, Fang A, Jin C, Zeng J, Song X, Guo X. Novel polymeric hybrid nanocarrier for curcumin and survivin shRNA co-delivery augments tumor penetration and promotes synergistic tumor suppression. *Front Chem.* 2020; *8*.
28. Santos TCD, Rescignano N, Boff L, Reginatto FH, Simões CMO, de Campos AM, Mijangos CU. Manufacture and characterization of Chitosan/PLGA nanoparticles nanocomposite buccal films. CarbohydrPolym. 2017;173:638.
29. Liu Q, Liu P, Ji T, Zheng L, Shen C, Ran S, Liu J, Zhao Y, Niu Y, Wang T, Dong J. The histone methyltransferase SUVR2 promotes DSB repair via chromatin remodeling and liquid-liquid phase separation. Mol Plant. 2022;15:1157.
30. Boon NJ, Oliveira RA, Körner P-R, Kochavi A, Mertens S, Malka Y, Voogd R, van der Horst SEM, Huismans MA, Smabers LP, Draper JM, Wessels LFA, Haahr P, Roodhart JML, Schumacher TNM, Snippert HJ, Agami R, Brummelkamp T. R. DNA damage induces p53-independent apoptosis through ribosome stalling. Science. 2024;384:785.
31. Pamujula S, Graves RA, Freeman T, Srinivasan V, Bostanian LA, Kishore V, Mandal TK. Oral delivery of spray dried PLGA/amifostine nanoparticles. J Pharm Pharmacol. 2004;56:1119.
32. Yang X, Ding Y, Ji T, Zhao X, Wang H, Zhao X, Zhao R, Wei J, Qi S, Nie G. Improvement of the in vitro safety profile and cytoprotective efficacy of amifostine against chemotherapy by pegylation strategy. BiochemPharmacol. 2016;108:11.
33. Lin X, Miao L, Wang X, Tian H. Design and evaluation of pH-responsive hydrogel for oral delivery of amifostine and study on its radioprotective effects. Colloids Surf B Biointerfaces. 2020;195:111200.
34. Zhang D, Zhong D, Ouyang J, He J, Qi Y, Chen W, Zhang X, Tao W, Zhou M. Microalgae-based oral microcarriers for gut microbiota homeostasis and intestinal protection in cancer radiotherapy. Nat Commun. 2022;13:1413.
35. Lu T-L, Sun W-g, Zhao W, Chen T. Preparation of amifostinepolylactide-co-glycolide microspheres and its irradiation protective to mouse through oral administration. Drug Dev Ind Pharm. 2011;37:1473.
36. Liu Y, Miao L, Guo Y, Yuan R, Li X, Wang X, Lin X, Tian H. Oral codelivery of WR-1065 using curcumin-linked ROS-sensitive nanoparticles for synergistic radioprotection. ACS BiomaterSci Eng. 2021;7:2496.
37. Cao J, Peng X, Li H, Ren L, Xu T, Sun K, Zhang Y, Li D. Ultrasound-assisted continuous-flow synthesis of pegylated MIL-101(Cr) nanoparticles for hematopoietic radioprotection. Mater SciEng C Mater Biol Appl. 2021;129:112369.
38. Swynnerton NF, Huelle BK, Mangold DJ, Ludden TM. A method for the combined measurement of ethiofos and WR-1065 in plasma: application to Pharmacokinetic experiments with ethiofos and its metabolites. Int J RadiatOncolBiol Phys. 1986;12:1495.
39. Utley JF, Seaver N, Newton GL, Fahey RC. Pharmacokinetics of WR-1065 in mouse tissue following treatment with WR-2721. Int J RadiatOncolBiol Phys. 1984;10:1525.
40. Smoluk GD, Fahey RC, Calabro-Jones PM, Aguilera JA, Ward JF. Radioprotection of cells in culture by WR-2721 and derivatives: form of the drug responsible for protection. Cancer Res. 1988;48:3641.
41. Lin X, Wang X, Tian H. Oral delivery of WR-1065 by ROS-responsive PEG-PCL nanoparticles for radioprotection. Colloids Surf A. 2020;599:124886.

42. Heger M, van Golen RF, Broekgaarden M, Michel MC. The molecular basis for the pharmacokinetics and pharmacodynamics of Curcumin and its metabolites in relation to cancer. Pharmacol Rev. 2014;66:222.
43. Hassaninasab A, Hashimoto Y, Tomita-Yokotani K, Kobayashi M. Discovery of the Curcumin metabolic pathway involving a unique enzyme in an intestinal microorganism. Proc Natl AcadSci U S A. 2011;108:6615.
44. Pontes-Quero GM, Benito-Garzón L, Pérez Cano J, Aguilar MR, Vázquez-Lasa B. Amphiphilic polymeric nanoparticles encapsulating Curcumin: antioxidant, anti-inflammatory and biocompatibility studies. Mater SciEng C Mater Biol Appl. 2021;121:111793.
45. Xie Y, Gong X, Jin Z, Xu W, Zhao K. Curcumin encapsulation in self-assembled nanoparticles based on amphiphilic palmitic acid-grafted-quaternized Chitosan with enhanced cytotoxic, antimicrobial and antioxidant properties. Int J BiolMacromol. 2022;222:2855.
46. Feng R, Song Z, Zhai G. Preparation and in vivo pharmacokinetics of curcumin-loaded PCL-PEG-PCL triblock copolymeric nanoparticles. Int J Nanomed. 2012;7:4089.
47. Song Z, Zhu W, Liu N, Yang F, Feng R. Linolenic acid-modified PEG-PCL micelles for Curcumin delivery. Int J Pharm. 2014;471:312.
48. Sahu A, Bora U, Kasoju N, Goswami P. Synthesis of novel biodegradable and self-assembling methoxy poly(ethylene glycol)-palmitate nanocarrier for Curcumin delivery to cancer cells. ActaBiomater. 2008;4:1752.
49. Zhang J, Li K, Zhang Q, Zhu Z, Huang G, Tian H. Polycysteine as a new type of radio-protector ameliorated tissue injury through inhibiting ferroptosis in mice. Cell Death Dis. 2021;12:195.
50. Matsuu-Matsuyama M, Nakashima M, Shichijo K, Okaichi K, Nakayama T, Sekine I. Basic fibroblast growth factor suppresses radiation-induced apoptosis and TP53 pathway in rat small intestine. Radiat Res. 2010;174:52.
51. Li K, Zhang J, Cao J, Li X, Tian H. 1,4-Dithiothreitol treatment ameliorates hematopoietic and intestinal injury in irradiated mice: potential application of a treatment for acute radiation syndrome. IntImmunopharmacol. 2019;76:105913.
52. Bhanja P, Norris A, Gupta-Saraf P, Hoover A, Saha S. BCN057 induces intestinal stem cell repair and mitigates radiation-induced intestinal injury. Stem Cell Res Ther. 2018;9:26.
53. Kim CK, Yang VW, Bialkowska AB. The role of intestinal stem cells in epithelial regeneration following radiation-induced gut injury. Curr Stem Cell Rep. 2017;3:320.
54. Liu W, Chen Q, Wu S, Xia X, Wu A, Cui F, Gu Y-P, Zhang X, Cao J. Radioprotector WR-2721 and mitigating peptidoglycan synergistically promote mouse survival through the amelioration of intestinal and bone marrow damage. J Radiat Res (Tokyo). 2015;56:278.
55. Lindemans CA, Calafiore M, Mertelsmann AM, O'Connor MH, Dudakov JA, Jenq RR, Velardi E, Young LF, Smith OM, Lawrence G, Ivanov JA, Fu YY, Takashima S, Hua G, Martin ML, O'Rourke KP, Lo YH, Mokry M, Romera-Hernandez M, Cupedo T, Dow L, Nieuwenhuis EE, Shroyer NF, Liu C, Kolesnick R, van den Brink AM. Interleukin-22 promotes intestinal-stem-cell-mediated epithelial regeneration. *Nature.* 2015; *528*: 560.
56. Nickoloff JA. Toward greater precision in cancer radiotherapy. Cancer Res. 2021;81:3156.
57. Han C, Liu Z, Zhang Y, Shen A, Dong C, Zhang A, Moore C, Ren Z, Lu C, Cao X, Zhang C-L, Qiao J, Fu Y-X. Tumor cells suppress radiation-induced immunity by hijacking caspase 9 signaling. Nat Immunol. 2020;21:546.
58. Nangia V, Siddiqui FM, Caenepeel S, Timonina D, Bilton SJ, Phan N, Gomez-Caraballo M, Archibald HL, Li C, Fraser C, Rigas D, Vajda K, Ferris LA, Lanuti M, Wright CD, Raskin KA, Cahill DP, Shin JH, Keyes C, Sequist LV, Piotrowska Z, Farago AF, Azzoli CG, Gainor JF, Sarosiek KA, Brown SP, Coxon A, Benes CH, Hughes PE, Hata AN. Exploiting MCL1 dependency with combination MEK + MCL1 inhibitors leads to induction of apoptosis and tumor regression in KRAS-mutant non-small cell lung cancer. Cancer Discov. 2018;8:1598.
59. Murray D, Milas L, Meyn RE. Radioprotection of mouse jejunum by WR-2721 and WR-1065: effects on DNA strand-break induction and rejoining. Radiat Res. 1988;114:268.
60. Jia J, Zhang L, Shi X, Wu M, Zhou X, Liu X, Huo T. SOD2 mediates amifostine-induced protection against glutamate in PC12 cells. Oxid Med Cell Longev. 2016;2016:4202437.

Publisher's note